2-17-2016

Resolving Fine Spectral Features in Lattice Vibrational Modes Using Femtosecond Coherent Spectroscopy

Feruz Ganikhanov
University of Rhode Island, fganikhanov@uri.edu

Adam Card
University of Rhode Island

Mohammad Mokim
University of Rhode Island

Citation/Publisher Attribution

Resolving Fine Spectral Features in Lattice Vibrational Modes Using Femtosecond Coherent Spectroscopy

Resolving fine spectral features in lattice vibrational modes using femtosecond coherent spectroscopy

A. Card, M. Mokim, and F. Ganikhanov

Resolving fine spectral features in lattice vibrational modes using femtosecond coherent spectroscopy

A. Card, M. Mokim, and F. Ganikhanov[a]

Department of Physics, University of Rhode Island, 2 Lippitt Road, Kingston, RI 02881, USA

We show resolution of fine spectral features within several Raman active vibrational modes in potassium titanyl phosphate (KTP) crystal. Measurements are performed using a femtosecond time-domain coherent anti-Stokes Raman scattering spectroscopy technique that is capable of delivering equivalent spectral resolution of 0.1 cm^{-1}. The Raman spectra retrieved from our measurements show several spectral components corresponding to vibrations of different symmetry with distinctly different damping rates. In particular, linewidths for unassigned optical phonon mode triplet centered at around 820 cm^{-1} are found to be 7.5±0.2 cm^{-1}, 9.1±0.3 cm^{-1}, and 11.2±0.3 cm^{-1}. Results of our experiments will ultimately help to design an all-solid-state source for sub-optical-wavelength waveform generation that is based on stimulated Raman scattering. © *2016 Author(s). All article content, except where otherwise noted, is licensed under a Creative Commons Attribution 3.0 Unported License.* [http://dx.doi.org/10.1063/1.4942478]

Precise information on fine structure and decay of Raman active modes is essential from both fundamental and device applications point of views. Time-domain studies provide direct information on decay and dephasing processes for vibrational modes and, for solid-state media, provide most valuable information as concerned parametric phonon interaction due to deformation potential anharmonicity. In frequency domain, dispersion of the corresponding nonlinear optical susceptibility is an essential charcateristic in order to get an insight into physics of intra- and interatomic groups interactions. In this paper we focus on an important nonlinear optical gain material that is used both as intracavity and external gain material in multi-wavelength laser devices. The attention has recently grown due to possible applications of efficient frequency converters in generating phase-locked frequency combs for attosecond waveform generation. Potassium titanyl orthophosphate KTiOPO$_4$ (KTP) is a widely known optical material that is particularly attractive for nonlinear optical applications. Because of its high nonlinear optical coefficient and its optical and mechanical stability, the crystal is used in laser sources as an optical frequency converter. Its large electro-optic coefficient, low dielectric constant and ion exchange properties also make it suitable for electro-optic[1] and waveguided laser devices.[2] The crystal was previously shown to be an efficient source for multi-wavelength pulse generation via stimulated Raman scattering (SRS)[3,4] or as a combination of SRS and efficient second order frequency conversion.[5] Renewed interest came with recent SRS experiments on high-frequency crystal vibrations that promised a pathway towards a solid-state sub-optical-cycle waveform source.[6–8] In other words, materials with high second and third order nonlinearity associated with several Raman active vibrations at high frequency range are of interest from the standpoint of generating a frequency comb that would ultimately support attosecond waveforms.[9] Knowledge of key properties of lattice vibrations is thus important in the light of the applications of this material as a nonlinear gain (of both second and third order) medium.

KTP's vibrational spectra are quite complex. The spectra consist of about 100 Raman active peaks as a result of the crystal's multiatomic unit cell. The complexity makes it difficult to perform comprehensive and unambiguous phonon line assignment, to precisely measure bandwidth and

---

[a]Corresponding author: fganikhanov@uri.edu

separation of individual Raman active peaks, as well as to estimate Raman cross-section for each individual phonon line. Even though the material has been known for more than three decades, detailed spectroscopic studies on its Raman active vibrations are relatively scarce.[10–12] The performed studies helped to elucidate contributions to Raman and infrared spectra from major atomic units within the primitive cell, as represented by TiO_6 octahedra and PO_4 tethrahedra. Also, important details concerning line assignments and their major characteristics were provided by the studies. However, the information ultimately proved to be contradictory and detailed spectral features of some peaks were not provided by these experiments. In particular, the first comprehensive Raman study of KTP[10] assigned peaks at around 818 cm^{-1} to the ν_1 symmetric stretching mode within slightly distorted PO_4 tetrahedra simply due to the fact that the line does not show up in the infrared reflectivity spectra. There are either two or three components spaced apart by approximately 16-40 cm^{-1} with linewidths within the 15-25 cm^{-1} range, depending on the vibrational mode symmetry. Another study characterized Raman peaks in the vicinity of 800 cm^{-1} as most likely belonging to TiO_6 octahedra vibrational modes of different symmetry, providing mode separations within 11-38 cm^{-1} and the linewidth range of 9.2-16.4 cm^{-1}.[11] A study that followed later stated that the Raman line detected at ~830 cm^{-1} is an intergroup (Ti-O-P) vibration, but provided no details on the detected linewidths and separations for the different peaks.[12]

At room temperature, the Raman spectroscopy of KTP has also been investigated from 10 to 1400 cm^{-1} [13,14] and also studied as a function of high pressure revealing the existence of two additional phase transitions near the critical pressures of 5.5 and 10 GPa.[15] Temperature dependent Raman scattering were studied[16,17] and found that no phonon mode coalesces to central peak near T_c and reported it as a sign of damped soft mode.[16] A study on polarized Raman spectra showed strongest phonon line located at 234 cm^{-1}.[18] It is worth mentioning that no experimental or theoretical study can be found which addresses phonon dispersion properties or mechanisms for phonon line decay. As was mentioned above, there is a motivation for a more detailed characterization of phonon vibrations in the material in the light of a search for an efficient solid-state media for a sub-optical-waveform source. Indeed, the crystal possesses several high-scattering cross-section phonon modes within energy range of 200-1000 cm^{-1}. The modes are conveniently spaced apart so that generation of a frequency comb, via SRS with intrinsically phase-locked spectral components, would provide multi-octave bandwidth to support sub-femtosecond pulses.

In this work, we present data on the decay of some of the KTP crystal phonon modes within 640-850 cm^{-1}. We reveal the fine structure of the vibrations by retrieving the vibrational system's response function and Raman spectra. Our data provide details on the crystal's complex vibrational spectra supported by important quantitative results. The data obtained for an unassigned vibrational mode at 820 cm^{-1} supports the conclusion that the modes decay noticeably slower when compared to high-frequency modes originating from vibrations of the main TiO_6 or PO_4 atomic groups. We attempt to explain our linewidth results within the framework of parametric phonon interaction due to the deformation potential anharmonicity.

Time-domain CARS spectroscopy is a valuable tool that enables probing the dynamics of elementary excitations in condensed matter. This technique monitors in time a degree of coherence within the lattice or molecular vibrations created by two ultrashort optical pulses at an earlier moment of time. Tracing the net coherence provides information on characteristic relaxation and dephasing processes. In our studies we employed three-color CARS geometry with widely tunable 110-150 fs pulses.[19,20] The experimental set up is schematically shown in Figure 1. The two pulses that are needed to coherently drive lattice vibrations within a sample's macroscopic volume are provided by synchronously pumped optical parametric oscillators (OPOs) running at 76 MHz. The OPOs utilize high parametric gain periodically poled lithium tantalate (PPSLT) crystals. The OPOs were simultaneously pumped by a split output of a high-power mode-locked Ti:sapphire oscillator tuned to 765 nm. Detailed OPO characteristics and performance were reported in our recent publications.[21,22] The OPOs with pulsed outputs at 970-1020 nm and 1050-1100 nm, served to coherently drive lattice vibrations with energies within 600-990 cm^{-1}. Another small part of the Ti:sapphire oscillator was delayed and served as a probe pulse. All of the three pulses were intrinsically synchronized, made to overlap in space, and focused by a high numerical aperture (NA~1.25)
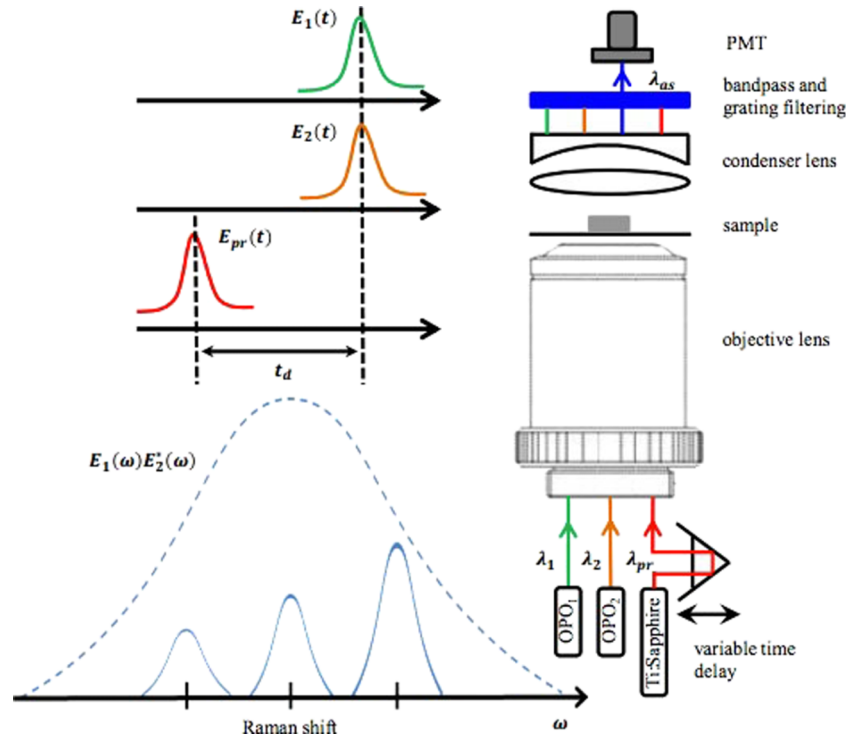
FIG. 1. Experimental diagram and layout for three-color time-domain CARS spectroscopy experiments that employ tunable optical parametric oscillators. Pair of transform-limited 110-150 fs pulses at λ_1 and λ_2 wavelengths are used to coherently drive Raman active vibrational modes in the vicinity of corresponding $\omega_1 - \omega_2$ frequency shifts. A pulse at λ_{pr}=765 nm is time delayed and probes the resulting coherent excitation at different delay times. CARS transients at anti-Stokes frequency are detected within five orders of magnitude. Polarizations of all the three beams were made parallel to each other and aligned within XY-plane of the KTP crystal under study.

objective lens. In the detection arm, we used a high numerical aperture (NA~0.9) condenser followed by a diffraction grating and a set of bandpass filters. This permitted efficient detection of the signal of interest on the background of other signals generated within the focal volume. A photomultiplier tube (PMT) with high gain and quantum efficiency (Hamamatsu model #R10699) was used to detect anti-Stokes signal photons at selected wavelengths. The PMT current output was digitized by a high-speed data acquisition card. Using this experimental arrangement, we can routinely detect CARS signals versus probe pulse delay times within five decades. The corresponding total power on the sample from the three beams does not exceed 15-20 mW. Other details and characteristics of the set up are described in our most recent work.[20] Figure 2(a) demonstrates sensitivity and the attainable time resolution using the experimental arrangement. In addition, using theoretical algorithms and owing to the experiment's great sensitivity, we can retrieve the vibrational system's response function and Raman spectra for several vibrational modes. The flux-grown KTP crystal used in the experiment was cut at ϕ=40° and θ=**9**0°. Polarizations of all the three beams were made parallel and aligned in XY-plane of the crystal. Thus, technically, all the four symmetry tensor components[10,11] are involved in Raman mode excitation and scattering processes during CARS.

Lattice dynamics in condensed matter is modeled as time-dependent behavior regarding the expectation value of molecular/atomic displacement amplitude under a driving force. This driving force consists of a pair of pulsed fields with an optical frequency difference matching the energy of vibration quanta.[23–25] Quantitatively, the scattering signal at anti-Stokes frequency ($S_{as}(t_d)$) can be expressed as the following:

$$S_{as}(t_d) = \zeta_0 \int_{-\infty}^{\infty} |\vartheta(t)|^2 \varepsilon_{pr}^2(t - t_d) dt. \tag{1}$$
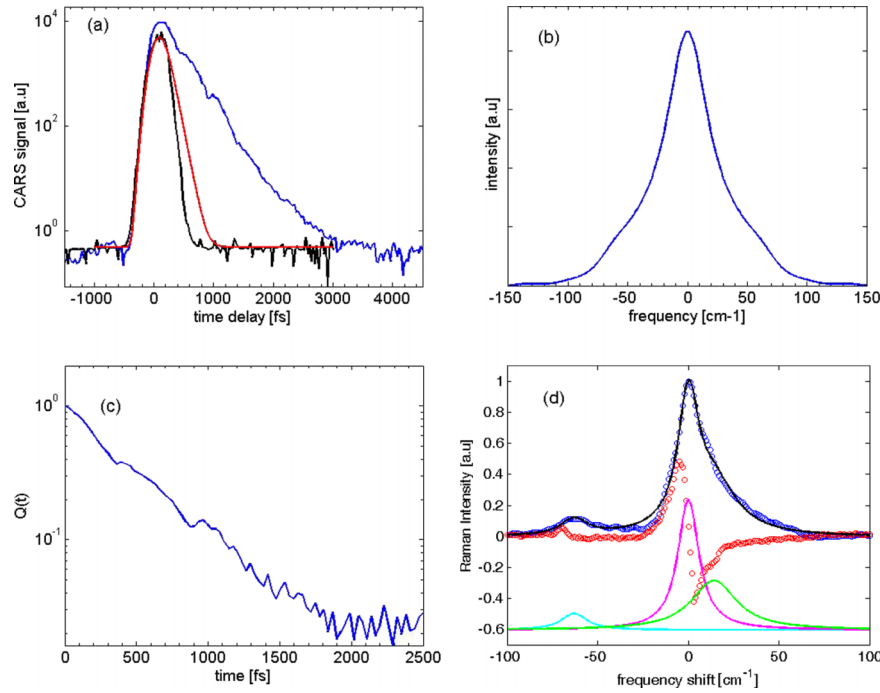
FIG. 2. (a) Time-domain CARS system instrument response obtained in quartz glass (black curve). Simulated CARS transient for Raman active vibrational mode with dephasing time T_2=150 fs (red curve). CARS transient detected in KTP crystal under the conditions specified below (blue curve). The broadband OPO pulses were tuned to 1020 nm and 1100 nm center wavelengths to coherently drive the main $\nu_1(A_{1g})$ high frequency Raman active mode at ~700 cm^{-1}. (b) CARS signal spectrum ($S_{as}(\omega)$) showing a narrower spectral feature on the background of a broadband pedestal corresponding to the transient signal's fast rise time. (c) Time-domain response function (g(t)) that was obtained by solving equations (1) and (2) using Fourier transform method. (d) Dispersion of real (red open circles) and imaginary (blue open circles) parts of the resonant third order optical nonlinearity ($\chi^{(3)}(\omega)$) in the vicinity of the coherently driven Raman active modes. The part corresponding to Raman spectra (i.e. $Im(\chi^{(3)}(\omega))$) is also shown fitted with solid black curve representation a sum of three Lorentz-shaped envelopes with bandwidths of 21 cm^{-1}, 17 cm^{-1}, and 25 cm^{-1} starting from the red shifted $\nu_2(E_g)$-mode (cyan color peak).

In the above equation, $\vartheta(t)$ and $\varepsilon(t)$ are normalized time-dependent envelopes for atomic displacement amplitude and probe pulse, respectively. This also implies that ζ_0 represents detected anti-Stokes signal at a zero delay. The ensemble averaged displacement amplitude is negligible well before the arrival of the driving pulse pair and one can find a solution for the dynamics equation in the form of correlation integral:

$$\vartheta(t) = \int_{-\infty}^{\infty} g(t' - t)\varepsilon_1(t')\varepsilon_2(t')dt'. \tag{2}$$

In the equation above, $g(t)$ represents the response function of the corresponding vibrational system to δ-pulsed driving fields. Both equations are of Fredholm type-I and can be solved using the Fourier transform method.[26] This is ensured by the correlation integral theorem and the fact that spectra and/or envelopes of $\varepsilon_1, \varepsilon_2, \varepsilon_{pr}$ pulses are known and can be measured. In the case when $\vartheta(t)$ is a real function, the response function $g(t)$ and its Fourier transform can be ultimately obtained. The condition holds true for many types of vibrational systems that do not involve diffusional phase shifting events. As a consequence, precise spectra and fine features in the vicinity of Raman active vibrations can be effectively resolved. Figure 2(a) shows an experimentally measured CARS signal versus delay time in the KTP crystal (open circles) under conditions that favor a coherently driven high-frequency (21.3 THz or ~710 cm^{-1}) Raman mode. For this case the OPO wavelengths were tuned to 1020 nm and 1098 nm respectively. The coherently driven Raman mode belongs to a main symmetric Ti-O bond stretching vibrations ($\nu_1(A_{1g})$) within the distorted TiO$_6$ octahedra. The

vibration has a relatively high damping rate so that the corresponding CARS signal decay time (∼250 fs) is comparable with pulsewidths used in our experiments. The crystal is of high quality and the only mechanism that results in the CARS signal decreasing versus time delay, is a decay of the coherently driven phonon into phonons of lower energy. From the measurement, a crude estimate can be made for the phonon lifetime ($T_1 \cong 495$ fs) and the corresponding phonon line bandwidth in ($\Delta v = 1/\pi c T_1 \cong 21$ cm^{-1}). A more rigorous analysis that concerns spectral domain information retrieved from the time-domain data is needed. For this particular case, the excitation and probe pulses can not be considered as δ-functions ($t_p \sim 3 \times T_1$) and an approach reported earlier by our group, described in Ref. 27, yields in somewhat distorted spectral data. Thus, equations above need to be solved in order to retrieve Raman spectra along with the dispersion of the real part of the associated resonant third order nonlinearity ($\chi^{(3)}(\omega)$). The Fourier transform ($S_{as}(\omega)$) of the measured time-dependent CARS signal is a first step in solving the equations. The corresponding result is shown in Figure 2(b). The spectrum is smooth, as high-frequency noise in the time-domain CARS signal has a relatively low spectral power density and is not visible on linear scale. The main characteristic of the spectrum is a broadband and high-intensity pedestal, associated with ultrafast signal rise-time. The pedestal masks a narrower spectral feature. The latter may reflect a slower decay rate due to the phonon decay process mentioned above. Knowing the measured probe pulse spectrum, ($I_{pr}(\omega) = FT(\varepsilon_{pr}^2(t))$), and applying the inverse Fourier transform operation, allows the collection of time-domain data on the coherent displacement amplitude ($\vartheta(t)$) at $|\vartheta(t)|^2 = FT^{-1}\left(\frac{S_{as}(\omega)}{I_{pr}(\omega)}\right)$. Further, having $\varepsilon_1(\omega), \varepsilon_2(\omega)$ available from OPO pulse autocorrelation and spectral measurements and a Fourier transform of $\vartheta(t)$, one can arrive to resonant third order nonlinearity ($\chi^{(3)}(\omega)$) spectra contained in real and imaginary parts of $g(\omega)$. Figure 2(c) shows the retrieved coherent amplitude function ($\vartheta(t)$) and the real and imaginary part of the resonant third order nonlinearity (Fig 2(d)) in the vicinity of the coherently driven $v_1(A_{1g})$ -phonon mode. The main peak's asymmetry is caused by the presence of two components with relative amplitude ratio of 26:11, bandwidths (FWHM) of 17.2±0.7 and 24±1.2 cm^{-1} and an energy separation of 16 cm^{-1} for the doublet. The difference in the bandwidths is explained by different damping rates for in-plane and along long axis vibrations within the TiO$_6$ octahedron.[10] A third component is also pronounced in the spectra with a position shifted to lower energies by 65 cm^{-1}. This mode has a different symmetry and represents $v_2(E_g)$ anti-phase stretching vibration within TiO$_6$ octahedra. The peak can be better resolved under condition when one of the OPOs is detuned to provide more efficient coherent excitation for the $v_2(E_g)$ mode. As a result, the time-dependent CARS signal exhibits a more pronounced quantum beats pattern. Using this arrangement, the spectral bandwidth of the $v_2(E_g)$ mode was determined to be 21.3±0.7 cm^{-1}. The obtained parameters for the main $v_1(A_{1g})$ doublet and for the $v_2(E_g)$ modes are in good general agreement with the referenced reports.[10,11] We must note, however, that consistent bandwidth and Raman shift data for the doublet components could not be found throughout Raman spectroscopy characterization studies of KTP crystal published in the past.[10–18,28–31] The result of fitting imaginary part of the resonant third order nonlinearity (i.e. Raman spectrum) using Lorentz-shaped multi-peak curves is also shown in Fig. 2(d) by solid lines with individual line details provided in the figure caption.

An unassigned phonon mode centered at ∼820 cm^{-1} is perhaps a better example of the complex nature of Raman active vibrations in the crystal. Figure 3(a) shows a CARS transient obtained for this case. The overall signal behavior shows quantum beats of at least two spectral components on the background of characteristic exponential decay with a noticeably longer time constant than for the $v_1(A_{1g})$ mode. Modeling of the time-domain behavior of CARS signals and the fitting of the experimental data require certain assumptions and use of multi-parametric fitting algorithms that do not have global minima. We have instead analyzed the obtained data by the approach that was outlined above. Fourier analysis of the signal unequivocally reveals a presence of a strong nonresonant signal on the background of weaker contributions from the clustered phonon mode. This proves the fact that the mode is noticeably weaker in its intensity when compared to the $v_1(A_{1g})$ and $v_2(E_g)$ modes. Retrieved Raman spectra (Im($\chi^{(3)}(\omega)$)) and data for the real part of the third order nonlinearity are shown in Figures 3(b) and 3(c) respectively. Three spectral components are involved in this case. They have energy separations of 18 cm^{-1} and 46 cm^{-1} and the values are
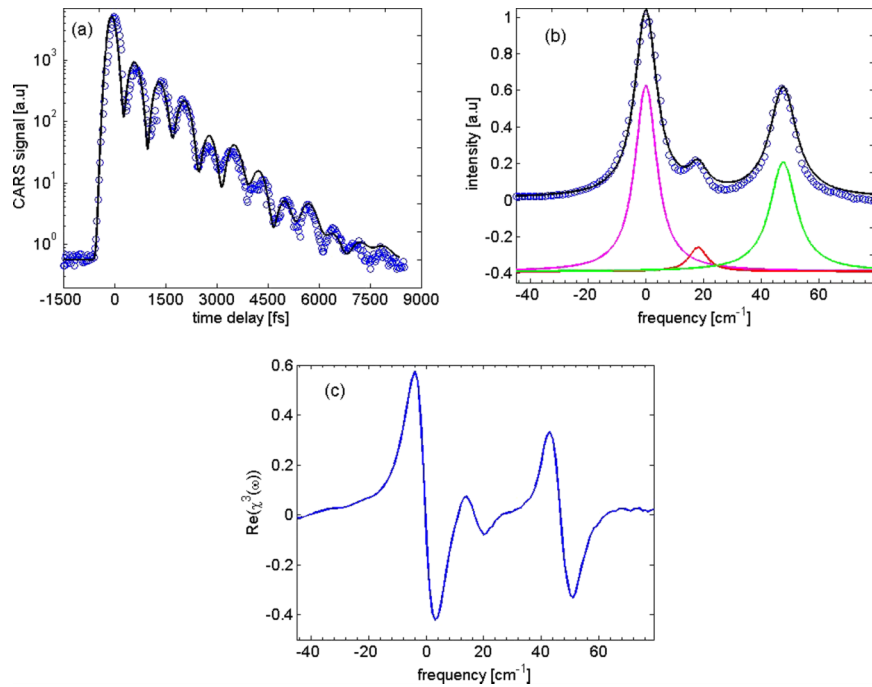
FIG. 3. (a) CARS transient (blue circles) obtained from KTP crystal when unassigned Raman active vibrational modes at ~820 cm^{-1} are coherently driven and probed. A proper wavelength combination was chosen for the OPOs (λ_1=967 nm and λ_2=1051 nm) so that the corresponding shift is targeted at its center. Simulated CARS signal (black curve) obtained under amplitude, damping rate, spectral shift parameter values for the vibrational modes using retrieved Raman spectra data. (b) Retrieved Raman spectra (blue curve), simulated Lorentz-shape curves for the three spectral components that yield in cumulative fitting curve (black). (c) Corresponding real part of the third order optical nonlinearity.

in relatively good agreement with spontaneous Raman scattering measurements. The latter provide the range of 20.4-29.0 cm^{-1} and 34.6−39.2 cm^{-1} for the corresponding two parameters.[11] Spectral component bandwidths obtained from our data are 9.1±0.4 cm^{-1}, 7.5±0.6 cm^{-1}, and 11.2±0.5 cm^{-1} for the three components compared to ranges of 10.2-12.6 cm^{-1}, 9.2-10.8 cm^{-1}, and 14.0-16.4 cm^{-1} respectively reported by spontaneous Raman spectroscopy study.[11] The spread for both parameters is dependent on particular experimental conditions (e.g. crystal axes orientations with respect to laser polarization) when different scattering tensor elements have been accessed within the measurements. And finally we report a component amplitude ratio of 46:5:31. The value is not available for comparison from spontaneous Raman spectroscopy studies Phonon line bandwidths are approximately two times narrower (i.e. the corresponding phonon decay rate is two times lower) when compared to the high frequency modes ($\nu_1(A_{1g})$ and $\nu_2(E_g)$) that are stronger in Raman scattering. We explain this by the fact that the latter modes have a variety of efficient overtone or combinational phonon decay channels within either of the TiO$_6$ or PO$_4$ groups, resulting in lower energy vibrations. Therefore, we think, that based on the fact that the investigated ~820 cm^{-1} mode has a significantly lower damping rate, the mode is not a vibration originating from either of the two main atomic groups and it is rather within Ti-O-P intergroup vibrations. The complex structure (i.e. presence of the triplet line) can be explained by shifted frequencies for vibrations of different symmetry within the group. Lower phonon damping rates (i.e. higher effective dephasing time T_2^*=T_1) makes up to a certain degree for the difference in the steady state SRS gain between the relatively weak mode at 820 cm^{-1} and the strong $\nu_1(A_{1g})$ and $\nu_2(E_g)$ vibrations. By using proper crystal orientation, it is possible to produce in SRS experiments (Stokes and anti-Stokes scattering) a nearly equal intensity and equidistant comb of frequencies that includes ~820 cm^{-1} mode. The comb can be used for ultrafast waveform synthesis.

In conclusion, we have demonstrated, using femtosecond time-domain coherent anti-Stokes Raman scattering spectroscopy, a resolution of complex Raman active vibrations in KTP crystal.

The Raman spectra retrieved from our measurements show several spectral components corresponding to vibrations of different symmetries with distinctly different damping rates. Relative amplitude ratio, energy shifts, and bandwidths for an unassigned optical phonon mode triplet centered at ~820 cm^{-1} have been reported. The mode is thought to belong to vibrations in the Ti-O-P intergroup within the crystal. Results of our experiments can be used to estimate stimulated Raman gain for different vibrational modes in the crystal.

[1] X. D. Wang, P. Basseras, R.J.D. Miller, and H. Vanherzelle, Appl. Phys. Lett. **59**, 519 (1991).
[2] Savatinova, I. Savova, E. Liarokapis, C.C. Ziling, V.V. Atuchin, M.N. Armenisek, and V.M.N. Passrok, J. Phys.D: Appl. Phys. **31**, 1667 (1998).
[3] V. Pasiskevicius, A. Fragemann, F. Laurell, R. Butkus, V. Smilgevicius, and A. Piskarskas, App. Phys. Lett. **82**, 325 (2003).
[4] V. Pasiskevicius, C. Canalias, and F. Laurell, App. Phys. Lett. **88**, 041110 (2006).
[5] Y.F. Chen, Opt. Lett. **30**, 400 (2005).
[6] L.L. Losev, J. Song, J. Xia, D. Strickland, and V. Brukhanov, Opt. Lett. **27**, 2100 (2002).
[7] M. Zhi and A. Sokolov, Opt. Lett. **32**, 2251 (2007).
[8] E. Matsubara, T. Sekikawa, and M. Yamashita, App. Phys. Lett. **92**, 071104 (2008).
[9] S. Baker, I. Walmsley, J.W.G. Tisch, and J.P. Marangos, Nature Photonics **5**, 664 (2011).
[10] G. E. Kugel, F. Brehatt, B. Wyncket, M. D. Fontanat, G. Marniers, C. Carabatos-Nedelect, and J. Mangin, J. Phys. C: Solid State Phys. **21**, 5565 (1988).
[11] G.H. Watson, J. Raman Spectrosc. **22**, 705 (1991).
[12] K. Vivekanandan, S. Setvasekarapandian, P. Kolandaivel, M.T. Sebastian, and S. Suma, Mater. Chem. Phys. **49**, 204 (1997).
[13] G.A Massey, T.M. Loehr, L.J. Willis, and J.C. Johnson, Appl. Optics **19**, 4136 (1980).
[14] V.M Garmash, D.N. Govorun, P.A. Korotkov, V.V Obukhovskii, N.I. Pavlova, and I.S Rez, Opt. Spectrosc. **58**, 424 (1985).
[15] G.A. Kourouklis, A. Jayaraman, and A.A. Ballamn, Solid State Commun. **62**, 379 (1987).
[16] Y.K. Voronki, V.A. Dyahov, A.B. Kudryavtsev, V.V. Osiko, A.A. Sobol, and E.V. Sorokin, Sov.Phys.-Solid State **31**, 1736 (1989).
[17] S. Fursawa, H. Hayasi, Y. Ishibashi, A. Miyamoto, and T. Sasaki, J.Phys.Soc.Jpn. **60**, 2470 (1991).
[18] C.S. Tu, A.R. Guo, R. Tao, R.S. Katiyar, R. Guo, and A.S. Bhalla, J. Appl. Phys. **79**, 3235 (1996).
[19] S. Yang, R. Wysolmerski, and F. Ganikhanov, Opt. Lett. **36**, 3849 (2011).
[20] S. Yang, S. Adhikari, L. Zhang, R. Wysolmerski, G Spirou, and F. Ganikhanov, Appl. Phys B: Lasers and Optics **111**, 617 (2013).
[21] K. Bhupathiraju, A. Seymour, and F. Ganikhanov, Opt. Lett. **34**, 2092 (2009).
[22] J. Rowley, S. Yang, and F. Ganikhanov, J. Opt. Soc. Am. B **28**, 1026 (2011).
[23] A. Laubereau, D. von der Linde, and W. Kaiser, Phys. Rev. Lett. **28**, 1162 (1972).
[24] A. Laubereau and W. Kaiser, Rev. Mod. Phys. **50**, 607 (1978).
[25] S. A. Malinovskaya, Opt. Lett. **33**, 2245 (2008).
[26] A. Jerry, *Introduction to Integral Equations With Applications*, 2nd ed. (John Willey and Sons, Inc., 1999).
[27] S. Yang and F. Ganikhanov, Opt. Lett. **38**, 4754 (2013).
[28] Ch. Ferrer, A. Segura, M.V. Andres, V. Munoz, and J. Pellicer, J. App. Phys. **79**, 3200 (1996).
[29] X. Liwen, C. Dawei, and N. Hongda, Chinese Phys. Lett. **1.6**, 225 (1989).
[30] M.J. Bushiri, V.P. M. Pillai, R. Ratheesh, and V.U. Nayar, J. Phys. Chem. Solids **60**, 1983 (1999).
[31] M.J. Bushiri and V.U. Nayar, J. Nonlinear Optic. Phys. Mat. **10**, 345 (2001).